

# A Polarized $^3\text{He}$ Gas Compression System Using Metastability-Exchange Optical Pumping

D.S. Hussey\*, D.R. Rich†, A.S. Belov‡, X. Tong, H. Yang,  
C. Bailey, X. Fei, C.D. Keith§, J. Hartfield, B. Neff, D. Allen, M. Flamini,  
B. Paturaliski, G. Hall, T. Black,¶W.M. Snow

*Department of Physics, Indiana University, Bloomington IN, 47408*

T.R. Gentile, W.C. Chen

*National Institute for Standards and Technology, 100 Bureau Dr., Stop 8461, Gaithersburg, MD 20899-8461*

G.L. Jones, E. Wildman

*Department of Physics, Hamilton College, Clinton, NY 13323*

September 8, 2004

## Abstract

Dense samples (10-100 bar-cm) of nuclear spin polarized  $^3\text{He}$  are utilized in high energy physics, neutron scattering, atomic physics, and magnetic resonance imaging. Metastability exchange optical pumping can rapidly produce high  $^3\text{He}$  polarizations ( $\approx 80\%$ ) at low pressures (few mbar). We describe a polarized  $^3\text{He}$  gas compressor system which accepts  $0.26 \text{ bar}\cdot\text{l}\cdot\text{h}^{-1}$  of  $^3\text{He}$  gas polarized to 70 % by 4 W of Nd:LMA laser power and compresses it into a 5 bar-cm target with final polarization of 55 %. The spin relaxation rates of the system's components have been measured using NMR and a model of the  $^3\text{He}$  polarization loss based on the measured relaxation rates and the gas flow is in agreement with a  $^3\text{He}$  polarization measurement using neutron transmission.

---

\*Current Address: National Institute for Standards and Technology, 100 Bureau Dr., Stop 8461, Gaithersburg, MD 20899-8461

†Current Address: Department of Physics, Wabash College, Crawfordsville, IN 47933

‡Current Address: Institute for Nuclear Research of Russian Academy of Sciences, 117312, Moscow, Russia

§Thomas Jefferson National Accelerator Facility

¶Current Address: Department of Physics and Physical Oceanography, University of North Carolina, Wilmington, NC 28403

# 1 Introduction

Dense samples of polarized  $^3\text{He}$  gas ( $\approx 5$  bar-cm) are utilized in several different fields of research including high energy physics, medical imaging, and neutron scattering. Several groups around the world have reported successfully using  $^3\text{He}$  in low-field magnetic resonance imaging (MRI) of the human lung [1, 2, 3, 4]. One can take advantage of the spin dependence of the  $^3\text{He}$  neutron absorption cross section to polarize or spin-analyze thermal neutrons [5, 6, 7, 8]. Since the  $^3\text{He}$  nuclear polarization is dominated by the unpaired neutron, it is used in nuclear and high energy physics to serve as a polarized neutron target [9, 10, 11]. Polarized  $^3\text{He}$  gas can also be used as a source for a polarized  $^3\text{He}$  atomic beam, which can be used as a surface scattering probe [12, 13].

To polarize  $^3\text{He}$  two different types of optical pumping are efficient, spin exchange optical pumping (SEOP) [14] and metastability exchange optical pumping (MEOP) [15]. In SEOP, one polarizes the  $5s$  electron of Rb atoms by optically pumping an optically thick vapor of Rb, which then transfers its electronic polarization to the  $^3\text{He}$  nucleus in atomic collisions. A practical advantage of this method is that one polarizes the  $^3\text{He}$  at the high densities needed for many applications. However the polarization transfer between the Rb and  $^3\text{He}$  is slow, taking  $\sim 1$  day to saturate the polarization of a  $100\text{-}500\text{ cm}^3$  volume of  $^3\text{He}$ . In contrast, MEOP polarizes  $^3\text{He}$  very quickly, allowing a  $100\text{ cm}^3$  target cell to be filled with polarized gas in about one hour. One reason for the faster production rate is that in MEOP one polarizes the  $2^3S_1$  metastable state, which quickly transfers its polarization to the nucleus in the same atom via the hyperfine interaction. The metastable state is typically produced by striking an RF discharge in the He, and so in practice the pressure of the polarized gas must be limited to  $\sim 1$  mbar to limit the polarization loss in the plasma environment caused by the discharge. So, one must compress the polarized  $^3\text{He}$  in order to have a sufficiently dense sample for many applications. The polarization preservation, the ratio of the polarization of the compressed gas to the initial polarization, is then a crucial quantity in determining the performance of the compression apparatus.

This paper describes the design, operation and characterization of the performance of a polarized  $^3\text{He}$  gas compression system. The mechanical compression apparatus is discussed in detail in Section 2. The  $^3\text{He}$  polarizer and the methods of polarimetry are described in Section 3. In Section 4, we report on relaxation rate measurements of the system's components and the polarization preservation. The polarization preservation measurements using neutron transmission, which includes a description of our polarized gas transport solenoid are described in Section 5. In Section 6, we compare the present performance of our system with the Mainz [16] and ILL [17] polarized  $^3\text{He}$  compressor systems, and discuss possible avenues for improving the performance of our compressor system.

## 2 Compression apparatus

### 2.1 Depolarization Mechanisms

The primary consideration in designing a polarized  $^3\text{He}$  compressor system is minimization of depolarization of the polarized gas. There are three contributions to relaxation, the dipole-dipole interaction between the nuclear spins, magnetic field inhomogeneities and wall relaxation. During atomic collisions, the dipole-dipole interaction results in a torque on the polarized nucleus and places a fundamental upper limit on the relaxation time ( $T1$ ) of a sample of polarized  $^3\text{He}$  gas and is given by

$$\frac{1}{T1_{dipole}} = \frac{p}{807} [\text{bar}^{-1}\text{h}^{-1}]. \quad (1)$$

at 300 K for pressure,  $p$ , measured in bar [18]. As polarized  $^3\text{He}$  diffuses in magnetic field gradients, in its rest frame it may feel time-dependent magnetic fields with frequency near the Larmor frequency resulting in a spin flip. Schearer *et al* [19] showed that the diffusion in magnetic field inhomogeneities causes a spin relaxation time

$$\frac{1}{T1_{field}} = \frac{2}{3} \left( \frac{1}{B_0} \frac{dB_r}{dr} \right)^2 \frac{\tau_c v_{thermal}^2}{\omega^2 \tau_c^2 + 1}, \quad (2)$$

where  $\tau_c$  is the mean time between collisions and  $\omega$  is the Larmor precession frequency. Assuming that  $\tau_c\omega \ll 1$ , one expects  $T_{field} \propto p$ , where  $p$  is the pressure of the gas. At a pressure of 1 mbar,  $T1_{field} = 10.6$  h due to field inhomogeneities  $(dB_r/dr)(1/B_0) = 10^{-4} \text{ cm}^{-1}$ , which is much longer than the  $T1$  of the plasma discharge in the optical pumping region, see Section 3.3.3. The relaxation due to interaction with the container surface is typically observed to be proportional to the surface to volume ratio [20]

$$1/T1_{wall} = \eta \frac{S}{V}, \quad (3)$$

where the constant of proportionality,  $\eta$ , depends on the sticking coefficient of He, the electronic and nuclear spin structure of the material and other possible surface phenomena that are not completely understood. A list of materials used in the compressor construction which come in contact with polarized  $^3\text{He}$  and their respective  $\eta$ 's is given in Table 1.

## 2.2 Description of the Apparatus

The entire compressor system (Figures 1 and 2) is immersed in a uniform magnetic field to suppress depolarization due to magnetic field gradients. The magnetic field is produced by a four coil system, constructed by Walker Scientific [21], based on the design of Franzen, *et al* [22]. The coils are powered by a HP 6674A power supply and produce a field of 0.1 mT A<sup>-1</sup>, with field gradients  $\leq 10^{-4} \text{ cm}^{-1}$  over a cylindrical volume 70 cm diameter by 70 cm long, rendering spin relaxation due to magnetic transverse field gradients negligible. The optical pumping cells (OPCs) and most of the connecting tubing were constructed from standard laboratory Pyrex glass. There are four OPCs, each 70 cm long with an inner diameter of 5 cm. A MKS Baratron Type 121A absolute pressure transducer measures the pressure in the OPCs. This gauge contains some magnetic materials, and is thus mounted  $\approx 20$  cm away from the OPCs. The OPCs are secured from impurities escaping the getter/purifier or released in outgassing by the remainder of the system by the presence of LN<sub>2</sub> cooled traps on either side of the OPCs.

A pair of piston compressors constructed entirely of 6061-T6 aluminum perform the compression.

An aluminum piston is connected by a threaded brass rod and a Unilat coupler to an Econo-Ram II (Schrader-Bellows) pneumatic drive cylinder. (The Unilat coupler absorbs both translational and rotational misalignments between the drive cylinder and the piston and is therefore superior to a universal joint.) A type 347 stainless steel (American Iron and Steel Institute) flexible bellows from Standard Bellows seals the drive shaft. Two Viton quad rings act to center the piston within the cylinder, and to prevent the flow of  $^3\text{He}$  into the rear of the compressors. Krytox, a low vapor pressure fluorinated grease, coats the inside surfaces of the cylinders. Fractional gas losses to the backside of the compressor through the quad rings were found to be  $\approx 10^{-5}$  per stroke. The end-caps of the compressors are aluminum Conflat flanges, with a titanium nitride coated knife-edge, and are sealed with an aluminum gasket. The inlet and outlet pneumatic valve seats are machined into the side of the Conflat flange and were designed to minimize the dead volume (DV) of the compressors [23]. The valves are constructed of phosphor-bronze bellows and valve heads. The first compressor (C1) has a 15 cm diameter and a 2.6 liter volume, with a piston stroke of  $\approx 15$  cm. The second stage compressor (C2) is 10 cm diameter, 0.75 liter volume, with a stroke of  $\approx 9.5$  cm. The compression ratio, which is the ratio of the total compressor volume to the dead volume,  $\kappa_{1(2)} = V_{C1(2)}/DV$ , was determined by measuring the pressure changes in the connecting tubing with the piston in the forward and withdrawn positions. These measurements yielded  $\kappa_{C1} = 176 \pm 12$  and  $\kappa_{C2} = 80 \pm 8$ .

In between the compressors sits the buffer cell (BC), a 1.2 liter Corning 1720 glass sphere. A completely non-magnetic ceramic pressure gauge by Bourdon-Sedeme measures the pressure in the BC. Compressed polarized gas accumulates in a storage cell (SC), constructed of either a borosilicate or aluminosilicate glass. Another non-magnetic ceramic pressure gauge measures the pressure in the SC. The storage cell detaches at a glass-to-glass o-ring seal, allowing it to be valved off and transported to the experimental area. Both the SC and BC are connected to the OPCs (and each other) via 6 mm Pyrex tubing enabling the measurement of the accumulated polarization by the optical polarimeter or the calibrated OPC-FID gauge, see Section 3.4.

A turbomolecular pump with a rotary vane forepump evacuates the compressor system. A cold

cathode gauge measures the pressure near the turbo and the typical base pressure at this point is  $1.8 \times 10^{-6}$  mbar. Due to the small conductance of the connecting tubing, the base pressure of the glassware is higher, as evidence by the weak discharge which can be maintained in the OPCs when the system is at the base pressure.

### 2.3 Construction and purification

The entire system was mounted on an aluminum optical breadboard . The Viton o-rings and quad-rings used throughout the device were baked at  $80^\circ\text{C}$  in a vacuum chamber to rid them of excess impurities before they were installed in the system. The compressor cylinders were clamped in place on the breadboard and all other components were assembled relative to the fixed compressors. A thin layer of Krytox grease was applied to the inside of the cylinders, and the respective pistons were inserted. Slight adjustments in the axial placement of the piston within the compressor could be made by adjusting the depth of the threaded brass rod which couples the piston to the drive cylinder. The flexible stainless steel bellows was welded to a mating piece and sealed to the rear Conflat flange with a Viton o-ring seal. The opposite end of the bellows is welded to a compression o-ring fitting, which seals the compressor back end on the outside of the drive rod and rotates to accommodate any rotational misalignment between the cylinder and the piston rod. Placement of the pneumatic drive (and hence, placement of the piston along the cylinder axis) was performed with the back-end under vacuum. In this way, the piston could be placed in its compressed position near the front face of the compressor with  $\approx 1$  mm accuracy.

After evacuating the system, the OPCs were then baked at  $110^\circ\text{C}$  for a total of 16 h to drive impurities from the walls. The system was then filled and flushed several times with  $^4\text{He}$ . First, the system was flushed for several hours with a continuous flow of  $^4\text{He}$  while the getter was slowly activated to  $375^\circ\text{C}$ . With the getter activated and at a constant temperature, the system was filled several times with a few mbar of  $^4\text{He}$ , then subsequently evacuated. To provide additional cleaning of the OPCs, a high voltage RF discharge was struck in the low pressure  $^4\text{He}$ . The discharge was

then examined using a Spectrascope spectrometer; impurities introduce a continuous background to the pure He discharge line spectrum.

## 2.4 Compression Cycle

To fill the storage cell with polarized  $^3\text{He}$ , gas is introduced into the OPC region. The flow of  $^3\text{He}$  is controlled by the bottle regulator pressure as well as a precision needle valve in conjunction with a stainless steel capillary (0.10 cm diameter by 7.62 cm long). The He gas is purged of impurities by passage through an Ultra Pure Systems two-stage getter and purifier. The getter and purifier (G/P) are encased in a stainless steel housing which was found to give a negligible magnetic field gradient in the nearby region. The getter is specified to reduce  $\text{H}_2\text{O}$ ,  $\text{O}_2$ ,  $\text{CO}$ ,  $\text{CO}_2$ ,  $\text{N}_2$  and  $\text{H}_2$  impurities to less than 10 parts-per-billion and the filter removes particles down to  $0.003\ \mu\text{m}$  in size with a retention efficiency of 99.999999%.

After passing through the G/P, the gas flows through a  $\text{LN}_2$  trap on its way into the OPCs. The gas is polarized in the last two cells (see Section 3), and flows through another  $\text{LN}_2$  trap before entering the first compressor. The timing sequence of C1 is shown in Figure 3. C1 opens to the OPCs for 3.5 s, allowing time for pressure equilibration. The inlet valve then closes, and the piston moves forward for 3.0 s. The outlet valve to the buffer cell then opens for 1 s, again allowing time for pressure equilibration. Finally, all valves close and the piston withdraws. C1 operates continuously (even during the buffer cell drain) until the storage cell has reached its set pressure. C2 is operated when the buffer cell reaches a set pressure. C2 has a similar valve sequence to C1, with the buffer cell replacing the OPCs and the storage cell replacing the buffer cell. C2 continues to operate until the pressure in the storage cell does not increase by more than a few percent, which typically takes 5 compressions. C2 is evacuated while the buffer cell is filled in order to remove the depolarized residual gas. The compression cycle ceases once the pressure in the storage cell reaches a set value.

### 2.4.1 Simulation Code

We constructed a computer simulation of the gas flow in the compressor based on the ideal gas law and the assumption that all volumes reach an equilibrium pressure before a valve closes. The only adjustable parameter is the gas flow rate which is determined by the fill time of the buffer cell. This code also calculates the expected polarization preservation by relaxing the polarized gas in each volume, as discussed in Section 4. The measured and simulated pressure in the OPCs, BC and SC from a typical fill are shown in Figure 4.

## 3 Polarizer and Polarimetry

### 3.1 Overview

Pure  $^3\text{He}$  or a 2:1  $^4\text{He}:$  $^3\text{He}$  mixture is polarized by metastability exchange optical pumping (MEOP). A weak RF discharge ( $\sim 50$  W), frequency  $\sim 10$  MHz, is struck in two of the OPCs by applying high voltage RF to four ring electrodes of opposite polarity, thus populating the metastable  $2^3S_1$  state of the He atom. Circularly polarized laser light at 1083 nm is introduced into the  $^3\text{He}$  along an axis parallel to the magnetic field axis. While there is a RF discharge, the nuclear polarization of the  $^3\text{He}$  is determined by measuring the degree of circular polarization of the 668 nm ( $3^1D_2 \rightarrow 2^1P_1$ ) light emitted from the discharge [24]. Additionally, we can measure the  $^3\text{He}$  nuclear polarization in the OPCs, BC and SC using free induction decay (FID) nuclear magnetic resonance.

### 3.2 Metastability Exchange Optical Pumping

In MEOP, circularly polarized light at 1083 nm excites the  $2^3S_1$  state to the  $2^1P_1$  states. The  $3^2S_1$  and  $2^1P_1$  states are split by the fine and hyperfine interactions, yielding a total of 9 different allowed transitions for  $^3\text{He}$ , labeled  $C1 - C9$  and 3 transitions for  $^4\text{He}$ , labeled  $D0 - D2$  [25]. The  $^3\text{He}$  transitions  $C8$  and  $C9$ , and the  $D0$  transition in  $^4\text{He}$  have been shown to produce the largest  $^3\text{He}$

polarizations [26, 27]. In polarizing pure  $^3\text{He}$ , circularly polarized light excites either the  $C8$  or  $C9$  transition, which depletes the metastable  $^3S_1$  state of one spin state. The nucleus is then polarized via the hyperfine interaction. The metastability is exchanged with ground state atoms in fast atomic collisions which leave the nuclear spin intact [15]. When using mixtures of  $^4\text{He}:^3\text{He}$ , the situation is a bit more complex. One pumps the  $D0$  transition of the  $^4\text{He}$  atom. The electronic polarization of the  $^4\text{He}$  metastable state is transferred to the  $^3\text{He}$  via collisions. Higher  $^3\text{He}$  polarizations have been observed [26] and expected based on rate calculations [25] when one polarizes a mixture of  $^4\text{He}:^3\text{He}$ , due to a more efficient absorption of the laser light by the  $D0$  transition as well as an increased ratio of metastable to ground state atoms [28].

### 3.3 Polarizer

#### 3.3.1 Nd:LMA Crystal

The krypton arc-lamp pumped neodymium doped lanthanum magnesium hexaluminate (Nd:LMA) [29] laser used for optical pumping emits linearly polarized light, has high power ( $\sim 10$  W free-running), a linewidth well matched to the 2 GHz Doppler absorption bandwidth of the He gas, and possesses several longitudinal modes within this bandwidth with good spectral overlap with the optical pumping transitions [30]. We use a Lee Laser Inc., series 700 continuous wave Yttrium Aluminum Garnet (YAG) laser, in which the Nd:YAG crystal is replaced by a Nd:LMA crystal anti-reflection coated at 1083 nm. The Nd:LMA crystal (4 mm-diameter, 79 mm-length, doped with 15% Nd) was purchased from Union Carbide and cut, polished and anti-reflection coated at 1083 nm by Virgo Optics. A particular trouble with this crystal is the potential for thermal lensing. Because of unavoidable thermal gradients in the crystal from external water cooling, the resulting radial change in the rod's index of refraction causes the rod to act as a converging lens, with a focal length that decreases with increasing radial thermal gradients. If the lamp current is sufficiently high, the focus can reside within the crystal, causing a drop in output power and an increased risk of damaging the crystal

from thermal stress [30]. To minimize this effect the ends were made concave with a 45 cm radius of curvature.

### 3.3.2 Laser Optics

To tune the beam and reduce the linewidth, two uncoated solid etalons are placed symmetrically in the laser cavity, 2.5 cm from each coupling mirror, in a manner similar to [27]. The laser is tuned by positioning the etalons at near-normal incidence and changing their refractive indices by controlling their temperatures inside copper enclosures that surround the etalons. Located behind the laser cavity is a Pyrex glass tuning cell containing either pure  $^3\text{He}$  or pure  $^4\text{He}$ . When tuned to a transition wavelength, the leakage light through the rear mirror is absorbed by metastable He atoms in the cell and a photodiode detects the subsequent spontaneous emission. When tuned to either C9 or D0 the typical output power is  $\sim 4$  W.

Since the light emitted from the Nd:LMA crystal is linearly polarized ( $>99\%$ ), the light which leaves the output coupler passes through a quarter wave plate to become circularly polarized. Over the approximately 4 m traveled by the laser light to the OPCs, the beam diverges enough to uniformly illuminate the cross-sectional area ( $20\text{ cm}^2$ ) of the pumping cells. The light passes through the last OPC and then through the third OPC after a series of 3 near-normal incidence reflections to minimize the loss of circular polarization. Polarizing in the two OPCs yields about a 5% increase in the  $^3\text{He}$  polarization as compared to polarizing in only one OPC.

### 3.3.3 Optical Pumping Rates and Maximum Polarization

The ultimate achievable polarization in the OPCs,  $P_{max}$ , is a compromise between the increased spin relaxation due to the RF discharge and the increased optical pumping rate from the increase in metastable population. The optical pumping rate also depends critically on the laser output power and tuning. To measure the pumping rate, the OPCs were filled with pure  $^3\text{He}$  and isolated from the rest of the compressor system. Circularly polarized laser light then passed through one

OPC, and the optical polarimeter continuously measured the polarization over a period of 90 s. The polarization accumulation vs. time is then fit to an exponential,

$$P(t) = P_{max}[1 - \exp(-t/\tau)], \quad (4)$$

to estimate the pumping rate,  $\tau$ . (It is known that the optical pumping is not an exponential process as the polarization approaches saturation [25, 27];  $\tau$  should therefore be viewed as an approximate parameter characterizing mainly the initial stage of the optical pumping process.) We have measured typical pumping rates of  $\sim 10^{19} \text{ s}^{-1}$  and have achieved  $P_{max} = 0.71 \pm 0.05$  for 1 mbar of pure  $^3\text{He}$  gas in the OPCs. As mentioned in Section 3.2, the maximum achievable polarization can be improved by using a mixture of  $^4\text{He}:^3\text{He}$ . Shown in Figure 5 is the pump rate as a function of the RF discharge strength (characterized by the relaxation rate) for three pressures of pure  $^3\text{He}$  in the OPCs. These data are in good qualitative agreement with those obtained in [27].

## 3.4 Polarimetry

### 3.4.1 Optical Polarimeter

One can measure the polarization of  $^3\text{He}$  in the RF-discharge by measuring the circular polarization of the light at 668 nm from the transition  $3^1D_2 \rightarrow 2^1P_1$ . Our polarimeter design is similar to that of [24]. The  $3^1D_2$  state is created in a fast atomic collision which does not perturb the nuclear polarization. The excited electron is polarized by the nucleus by the hyperfine interaction. The degree of circular polarization is pressure dependent due to atomic collisions, and the pressure calibration factors have been measured in pure  $^3\text{He}$  [24] with a relative standard uncertainty of 2 %. In mixtures of  $^4\text{He}:^3\text{He}$  it is assumed that the measured degree of circular polarization scales with the mole fraction of  $^3\text{He}$ .

There are some systematic effects associated with the optical polarimetry method. Gas impurities may either absorb 668 nm light from the  $^3\text{He}$  and/or emit uncircularly polarized light near 668 nm, thereby increasing the background. The RF discharge itself causes relaxation with a  $T_1 = 10 \text{ s} - 100 \text{ s}$ ,

depending on the discharge strength. We also found that the initiation of the discharge can decrease the polarization by 15-30%, resulting in an unknown systematic error in later interrogation of the  $^3\text{He}$  polarization. Hence, we did not use the optical method to measure the polarization of the  $^3\text{He}$  in the BC or SC. However, we did use the optical method to calibrate the FID gauges discussed below as well as measure the polarization in the OPCs during compression.

### 3.4.2 Free Induction Decay

In order to measure the  $^3\text{He}$  polarization in the BC and SC, we used a portable nuclear magnetic resonance, free induction decay (FID) [31] device described in detail in [32, 33] and sketched in Figure 6. A short RF-pulse ( $\sim 1$  ms) with frequency ( $\omega_p$ ) near the Larmor frequency ( $\omega_L$ ) tips the  $^3\text{He}$  spin through an angle  $\alpha$ . The subsequent precession of the transverse component of the magnetization around the static magnetic field produces an oscillating magnetic field at the Larmor frequency, which is detected by the same coil after the RF pulse. The induced voltage is sent to a lock-in amplifier, whose reference frequency is that of the RF pulse,  $\omega_p$ . The beat signal of frequency  $\omega_b = |\omega_L - \omega_p|$  decays nearly exponentially with a time ( $T_2 \sim 10$  ms) due to diffusion of the nuclei out of the coil's sensing volume and magnetic field gradients [34]. Since the drive/pick-up coil is smaller than the sampling volume, the measurements do not benefit from motional narrowing at low pressures [35] and diffusion causes a nonlinear pressure dependence in the FID measurement (see Figure 8). In order to reduce the effects of diffusion on the FID measurement in the OPCs, we constructed a coil which was nearly twice the r.m.s. displacement of the gas atoms during the time of measurement ( $\langle x_{rms} \rangle \approx 5.5$  cm for 10 ms at 1.3 mbar). With this coil, we have been able to measure a FID signal with a signal to noise ratio of 3:1 in the OPCs with pure  $^3\text{He}$  at pressures as low as 1 mbar. FID measurements in the BC and SC are easier as the density of polarized nuclei is higher and the mean displacement is much shorter. For typical pressures in the BC (65 mbar) and SC (1 bar),  $\langle x_{rms} \rangle \approx 1.5$  cm and 0.4 cm, respectively for a 40 ms measurement. As one can see in Figure 7 the  $T_2$  for the higher pressures is much longer, with a good signal-to-noise ratio.

### 3.4.3 FID Calibration

The OPC-FID signal was calibrated using the optical polarimeter, using the peak-to-peak voltage difference between the first two periods of the beat signal, denoted by  $\Delta_{AB}$  and  $\Delta_{BC}$ . To calibrate the OPC FID-NMR gauge, pure  $^3\text{He}$  gas at pressures ranging from 1.0 mbar to 2.6 mbar was polarized in the OPCs. For the 2:1  $^4\text{He}:^3\text{He}$  mixtures, only two pressures (5.0 mbar and 2.7 mbar) were used. Once saturation was reached, the RF-discharge was extinguished and the FID-NMR signal was taken. The  $^3\text{He}$  polarization was related to the peak-to-peak differences via:

$$\Delta_{AB,BC} = \kappa_{AB,BC} p P_{^3\text{He}}, \quad (5)$$

where  $p$  is the pressure,  $P$  is the polarization and  $\kappa$  is the calibration coefficient, with units  $\text{mV}\cdot\text{mbar}^{-1}$ . Figure 8 shows the results of the OPC-FID gauge calibration. As one can see from Figure 8a, the raw FID signal is linearly proportional to the polarization as measured by the optical polarimeter and correctly extrapolates to zero. Also from the FID signal versus pressure curve, Figure 8b, one sees that at low pressure the signal is not linearly proportional to the pressure, as was discussed in Section 3.4.2.

To calibrate the BC-FID gauge, we filled the buffer cell with pure, polarized  $^3\text{He}$  to 65 mbar using a truncated version of the compression scheme outlined above. After filling the BC, the OPCs were evacuated and isolated from depolarizing portions of the system (see Section 4). Gas at 2 mbar pressure was bled into the OPCs by filling the tubing connecting the OPCs and the BC. We chose 2 mbar for an improved signal to noise ratio with OPC-FID gauge. There are systematic effects in the polarization measurement in flowing the gas from the BC to OPC region from depolarization of the gas in the Pyrex tubing which preferentially flows into the OPC. Briefly opening the valve connecting C1 and the BC before bleeding gas to the OPC, produces a 5 % to 10 % increase in the measured polarization and therefore produces a transient effect. Depolarization in the glass between the BC and OPC is negligible ( $\sim 1\%$ ). The SC-FID gauge was calibrated using the neutron transmission data discussed in Section 5.3.

## 4 Relaxation time measurements

### 4.1 Optical Pumping Cells

To measure the relaxation time in the OPCs, we polarized gas at 2.0 mbar for 15 min to allow the entire volume of the OPCs to equilibrate, extinguished the RF discharge, turned the laser off and measured the polarization with the OPC-FID gauge over a period of a few hours. The measured relaxation time of  $T1_{OPC} = 150$  min for the OPCs without a discharge in the isolated configuration is negligible compared to the relaxation due to the discharge  $\sim 100$  s.

### 4.2 Compressors

The relaxation time of C1 was measured by introducing polarized gas from the BC into C1, allowing the gas to remain in either the compressed or uncompressed state. The gas was introduced into the OPCs and its polarization measured by the OPC NMR-FID gauge. The relaxation times reported in Table 3 are corrected for the relaxation time of the buffer cell. By this method we measured the relaxation time in the withdrawn position to be  $T1_{C1,uc} = 60$  min and in the forward position to be  $T1_{C1,c} = 3$  min. The change in the relaxation rate is consistent with the change in the surface to volume ratio for the two piston positions.

To measure the same quantities for C2, a different scheme was necessary, as C2 is not directly connected to the OPCs. Polarized  $^3\text{He}$  gas from the BC was introduced into C2 and remained in the compressed or uncompressed state. The gas was then reintroduced to the BC and the polarization measured by the BC NMR-FID gauge. In order to extract  $T1_{C2,uc(c)}$  from these polarization measurements, we assumed that the measured FID signal had the following time dependence in the uncompressed state:

$$FID(t) = \frac{FID(t=0)}{V_{BC} + V_{C2}} e^{-(t-t_{uc})/T1_{BC}} (\times) \\ (V_{BC} e^{-t_{uc}/T1_{BC}} + V_{C2} e^{-t_{uc}/T1_{C2,uc}}), \quad (6)$$

where  $t_{uc(c)}$  is the time the polarized  $^3\text{He}$  spent in the uncompressed (compressed) state. The FID signal has a similar form for the compressed state by replacing  $t_{uc}$  with  $t_c$ . Since  $T1_{BC}$  (see section 4.3) and  $V_{C2}, V_{BC}$  (see section 2.2) were measured independently, it is possible to infer  $T1_{C2,uc(c)}$  from the data. The volume weighting assumes no gas loss during compression and that the gas has sufficient time to mix. These are reasonable assumptions given the measured gas loss per stroke of C2 (Section 2.2) and the root mean square displacement of 7.7 cm after 1 s at 65 mbar. Shown in Figure 9 is the FID signal as a function of  $t_{uc(c)}$ . From these fits, and including the time the piston moves forward, it was found that  $T1_{C2,uc} = 2250 \pm 90$  s and  $T1_{C2,c} = 190 \pm 43$  s. These  $T1$ 's scale with the change in surface to volume ratio of the two piston states. Additionally, when compared with the  $T1$ 's obtained for C1, they correctly scale with the S/V of the two compressors.

### 4.3 Buffer Cell

The buffer cell's relaxation time was measured using the BC-FID gauge at 54, 65 and 171 mbar and with the valve to the ceramic gauge opened and closed and found  $T1 = (6 \pm 1)$ , independent of pressure. This is consistent with our estimate of 6 h based on the typical uncoated 1720  $T1 \approx 20$  h, the S/V of the Pyrex tubing, and their relative volumes.

### 4.4 Storage Cells

We have mainly used a Rb coated GE 180 glass cell named "Orion", which is cell #13 in [36]. The Rb coating is known to increase a cell's  $T1$  [37], with SEOP cells with 1 bar of  $^3\text{He}$  obtaining  $T1 \leq 600$  hrs [36]. At a pressure of 0.933 bar in isolation from the compressor system, Orion's  $T1 = 210 \pm 10$  h, consistent with the results of [36].

### 4.5 Capillary Connecting Tubing

In an attempt to measure the systematic polarization loss in bleeding gas from the SC to the OPC due to the connecting tubing (CT), we measured the  $T1$  of Orion in different configurations in order

to understand the effects of pressure and the exposure to the CT on  $T1$ . The CT has a high S/V ( $\approx 20 \text{ cm}^{-1}$ ) and will thus have a short, pressure independent  $T1$ . We measured the relaxation at two different pressures, 170 and 650 mbar, with a mixture of 2:1  $^4\text{He}:$  $^3\text{He}$ , with Orion isolated and exposed to the CT. For both pressures, the isolated  $T1 \approx 200$  h. In the exposed state, when the polarized gas can diffuse to Pyrex regions with  $S/V \approx 20 \text{ cm}^{-1}$ ,  $T1_{eff}$  scales linearly with pressure with  $T1(170 \text{ mbar}) = (8.6 \pm 1.1) \text{ h}$  and  $T1(650 \text{ mbar}) = (32 \pm 1) \text{ h}$ . The pressure dependence suggests that the gas is diffusing to a region with a short  $T1$ . We have not been able to clearly identify the source of this depolarization. The fast relaxation in the first few cycles of C2 dominates the SC contribution to the polarization preservation. By shortening this tubing, or by more quickly achieving higher pressures in the SC, the relaxation in the SC would be dominated by the wall relaxation.

## 5 Polarization Preservation

We identify the polarization preservation as one relevant measure of performance of the compressor.

We define the polarization preservation as:

$$f_{BC} = \frac{P_{BC}}{P_{OPC}}, \quad f_{SC} = \frac{P_{SC}}{P_{OPC}}, \quad (7)$$

where  $P_x$  is the polarization of the  $^3\text{He}$  in the denoted volume. In order to estimate the expected polarization preservation, we measured the  $T1$  of polarized  $^3\text{He}$  in every major component of the compressor system. Using the measured relaxation rates, we have calculated the expected polarization preservation by a rough estimate and by using the simulation discussed in Section 2.4.1.

### 5.1 Preservation Estimate

Polarized  $^3\text{He}$  spends an average of 3.2 s in the uncompressed state and 1 s in the compressed state of C1. If we assume that the relaxation rate changes linearly according to the surface to volume ratio as the piston moves from the withdrawn to forward positions, then the polarization as a function of

time during the motion of the piston can be expressed as:

$$P(t) = P(0) \left( 1 - \frac{\Delta\tau}{\tau_{C1,W}\Delta t} \right)^{\frac{\Delta t}{\Delta\tau}}, \quad (8)$$

where  $\Delta t$  is the compression time and  $\Delta\tau = \tau_{C1,W} - \tau_{C1,F}$ . Combining the three relaxations, we find  $\left(\frac{P}{P_0}\right)_{C1} = 0.99$ . Performing the same calculation for C2 yields  $\left(\frac{P}{P_0}\right)_{C2} = 0.99$ . It takes approximately 15 min for the buffer cell to reach a pressure of 65 mbar. Since the pressure increase is approximately linear, the preservation for the first filling of the buffer cell is

$$\left(\frac{P}{P_0}\right)_1 = \exp\left(-\frac{\Delta t_{BC1}}{2T1_{BC}}\right), \quad (9)$$

where  $\Delta t_{BC,1} = 15$  min. Since the buffer cell is not emptied during C2's operation, the polarization in BC before the  $n$ th C2 operation is given by:

$$\left(\frac{P}{P_0}\right)_n = \frac{p_{n \min}}{p_{n \max}} \left(\frac{P}{P_0}\right)_{n-1} \exp\left(-\frac{\Delta t_{BC,n}}{T1_{BC}}\right) + \frac{p_{n \max} - p_{n \min}}{p_{n \max}} \exp\left(-\frac{\Delta t_{BC,n}}{2T1_{BC}}\right), \quad (10)$$

where  $p_{n \max(\min)}$  is the pressure before (after) C2 operates. Typically,  $p_{\max} = 65$  mbar and  $p_{\min} = 20$  mbar. So, for 4 cycles,  $\left(\frac{P}{P_0}\right)_{BC} = 0.95$ . If we assume that gas is linearly accumulated in the SC over 1 hour, we expect

$$\left(\frac{P}{P_0}\right)_{SC} = \exp(-\Delta t_{SC}/2T1_{SC}) = 0.935. \quad (11)$$

From these calculations, we estimate the polarization preservation after filling the buffer cell to 65 mbar to be  $f_{BC} = 0.94$  and for filling the storage cell to 1 bar,  $f_{SC} = 0.87$ .

## 5.2 Preservation Simulation

Using the code mentioned in Section 2.4.1, the polarization preservation after filling the SC is more accurately calculated by using the measured relaxation rates, the residence time in every volume in which polarized gas flows as well as using the actual pressures in each volume. Based on the results of Section 4.5 a pressure dependent  $T1_{SC}$  was incorporated in the calculation. Since the simulation reliably models the time dependence of the pressures in the various volumes (see Figure 4) we

are confident that the times used for the polarization relaxation simulation are correct. Based on these simulations, we expect  $f_{BC} = 0.92$  and  $f_{SC} = 0.83$  for pressures of 65 mbar and 1000 mbar, respectively for a typical operating flow rate of  $0.22 \text{ mbar}\cdot\text{l}\cdot\text{s}^{-1}$ , which gives an average pressure in the OPCs of  $\langle p_{OPC} \rangle = 2 \text{ mbar}$ .

### 5.3 Preservation Measurement

**Polarization of Optical Pumping Cells** To determine  $f_{BC}$  and  $f_{SC}$ , a definition of  $P_{OPC}$  is necessary. Since the gas flows, a pressure gradient necessarily exists and the pressure gauge will record a higher pressure than exists in the OPCs. The simulation code is used to correct the measured pressure and polarization calibration coefficients. The pressure correction is  $\approx 10\%$  while the polarization correction is  $\approx 2\%$ . The average OPC polarization,  $\langle P_{OPC} \rangle$  is found by:

$$\langle P_{OPC} \rangle = \frac{\langle p_{OPC} P_{OPC} \rangle}{\langle p_{OPC} \rangle}, \quad (12)$$

where  $P_{OPC}$  and  $p_{OPC}$  are the corrected OPC polarization and pressure, respectively. The pressure weighting accounts for the number of polarized nuclei transferred from the OPC to the BC per stroke.

#### 5.3.1 Buffer Cell

We measured the polarization preservation after filling BC to 65 mbar for different average pressures in the OPCs using pure  $^3\text{He}$  and the results are shown in Figure 10. The average measured preservation of  $0.92 \pm 0.05$ , is in excellent agreement with our expectations given above in Section 5.2.

#### 5.3.2 Storage Cell

To eliminate uncertainties in the polarization measurement introduced by flowing the gas from the SC to the OPCs, the final polarization in SC was measured using neutron transmission through Orion filled with polarized gas. The total neutron transmission through the  $^3\text{He}$  and the glass cell is given by [38]

$$T(\lambda) = T_e \exp(-nl\sigma_0) \cosh(nlP_{^3\text{He}}\sigma_0(\lambda)), \quad (13)$$

where  $T_e$  is the neutron transmission through the empty glass cell,  $n$  is the  $^3\text{He}$  number density,  $l$  is the length of the  $^3\text{He}$ , and  $\sigma_0(\lambda)$  is the wavelength dependent neutron absorption cross-section. By measuring three sets of transmission data, through the polarized cell, the depolarized cell and the empty cell, one can unambiguously determine the  $^3\text{He}$  polarization.

Polarized gas is transported to the neutron scattering facility in a battery powered transport solenoid. The solenoid is wound on a 31.4 cm diameter aluminum cylinder and is 53 cm in length. There are two sets of ultra low carbon steel  $\mu$ -metal shielding from Amuneal Manufacturing Corp, with a maximum permeability of  $\mu = 3000$  surrounding the solenoid to reduce external magnetic fields in the solenoid. The inner (outer) shield is 32.4 cm (40.6 cm) in diameter and is 56.5 cm (60.0 cm) in length and both are 1.27 mm thick. The shields also have end-caps with 10 cm diameter holes so a neutron beam can pass unattenuated. An estimate for the shielding factor for a double shield is given by:

$$A = 1 + A_i + A_o + A_i A_o (1 - (RO_i/RI_o)^2) \quad (14)$$

where the subscript  $i(o)$  stands for inner(outer) shield,  $RI(RO)$  is the inner(outer) radius of a shield, and the individual shielding factor is given by  $A_x = (\mu/4)(1 - (RI/RO)^2)$  [39]. Ignoring the effects of the holes in the end-caps, and assuming the maximum permeability this arrangement of  $\mu$ -metal shielding gives an estimated shielding factor of 60. The inner end-caps reroute the solenoid's field through the inner shielding, thus reducing stray fields that may leak into a sample area. We constructed a 3-dimensional magnetic field mapping system capable of mapping field gradients above  $1 \times 10^{-4} \text{ cm}^{-1}$ . The field mapping system measures the vectorial magnetic field with a Lakeshore triple axis probe. The probe is translated in 3 orthogonal directions with worm gear translators and is controlled through a Labview interface. The maximum volume that can be mapped with this system is  $\approx 1 \text{ m}^3$ . With this mapping system, the measured field gradients in the center region of our shielded solenoid  $\approx 3 \times 10^{-4} \text{ cm}^{-1}$ , yielding a  $T1_{field} \approx 1200 \text{ h}$  at a pressure of 1 bar.

Orion was filled to 1.22 bar with a 2:1  $^4\text{He}:$  $^3\text{He}$  gas mixture from Spectra Gases with a 5%

relative uncertainty in mixture ratio. The average polarization in the OPCs during the fill was  $\langle P_{OPC} \rangle = 0.56 \pm 0.03$ . Orion, was then placed in the transport solenoid and then driven in a car to POSY 1, the polarized neutron reflectometer at IPNS at Argonne National Laboratory in Argonne, IL. Six hours after filling, Orion was installed on the beamline (see Figure 11), and a power supply was connected to the transport solenoid to ensure a constant field while acquiring the neutron transmission through the polarized cell. We measured the transmission of the unpolarized neutron beam through the polarized cell ( $T_N$ ) in 14, 1 h long data sets. The  $^3\text{He}$  was then depolarized, and a 10 h transmission run ( $T_0$ ) was collected. Orion was then evacuated, and the empty cell's transmission ( $T_e$ ) was measured.

To determine the initial  $^3\text{He}$  polarization, we first determine the thickness of the  $^3\text{He}$  from  $T_0/T_e$ , shown in Figure 12. From this fit, the optical thickness was determined to be  $nl = 5.040 \pm 0.004$  bar-cm. By fitting  $\cosh[P_{^3\text{He}}nl\sigma(\lambda)]$  to the averaged  $T_N$ 's, normalized by  $T_0$ , the average  $^3\text{He}$  polarization during data collection period is obtained, see Figure 13. The  $\langle P_{^3\text{He}}(t) \rangle$  data was then fit by the time averaged polarization:

$$\langle P(t) \rangle = \frac{T_1}{\tau} \exp(-t/T_1)[1 - \exp(-\tau/T_1)], \quad (15)$$

where  $\tau$  is the length of the averaging period and  $t$  is time at the beginning of the data collection. This fit gave  $T_1 = 100 \pm 10$  hours. Once  $T_1$  was determined, the initial polarization of Orion was determined to be  $P_{SC}(t = 0) = 0.464 \pm 0.046$ . This  $P_{SC}$  assumes that there were no losses in polarization during the transfer of Orion from the compressor's holding field to the transport solenoid, but does include the relaxation of Orion while on the compressor during the 39 minutes between completion of the fill and transfer to the transport solenoid.

Taking the ratio of  $P_{SC}$  and  $P_{OPC}$ , we find for the polarization preservation,  $f_{SC} = 0.81 \pm 0.09$ , which is in agreement with the expected preservation of 0.83 based on simulation. We conclude that the polarized gas compression system is operating at the theoretical limit to the polarization preservation which is based solely on the system components' relaxation rates.

## 6 Conclusions

### 6.1 Comparison with current Mainz and ILL $^3\text{He}$ compressor systems

Both the current Mainz and ILL  $^3\text{He}$  compressor systems are of larger scale than our system, about an order of magnitude larger in OPC volume and total flow rate. However, the original system described in [40] is of similar scale to our compression system. The current polarized  $^3\text{He}$  system constructed by the Mainz group consists of five 2.4 m long optical pumping cells. Their system has one compressor, fabricated entirely of Titanium and compression is performed by a hydraulic system. They incorporate an intermediate buffer cell, and have found that this volume is the dominant source of depolarization. They polarize the  $^3\text{He}$  with two 15 W Yb fiber lasers and can achieve a maximum steady state polarization of  $84\pm 2\%$  [41]. With a flow rate of  $1 \text{ bar}\cdot\text{l}\cdot\text{h}^{-1}$ , their systems yields an OPC polarization of 75%, and a final polarization of 70.5% [16]. The first polarized  $^3\text{He}$  compressor system at the ILL was initially commissioned in 1996 [42] and was based on the Mainz system [40]. Their current system consists of five optical pumping cells, with a total volume of 39 l, maintained at 1 mbar. They employ a single compressor body (5.2 l in volume), machined entirely of Titanium and the separation of the piston and flange is finely tuned to  $\approx 100 \mu\text{m}$ . Compression is performed by a hydraulic system in which the buffer cell is filled several times before filling the storage cell [43]. They are using several 4 W, 2 GHz linewidth Yb fiber laser, with a flow rate of  $1.4 \text{ bar}\cdot\text{l}\cdot\text{h}^{-1}$ , resulting in a final  $^3\text{He}$  polarization of  $\approx 60\%$  [17].

### 6.2 Summary of our polarized $^3\text{He}$ compressor system

Using a total gas flow rate of  $0.8 \text{ bar}\cdot\text{l}\cdot\text{h}^{-1}$  (for a 2:1  $^4\text{He}:\text{}^3\text{He}$  mixture), our measured polarization preservation of  $0.81 \pm 0.09$  agrees with the limit of 0.83 which is based on the system components' relaxation rates. We have identified the relaxation in the BC and SC connecting tubing as the main source of polarization loss. The grease in the aluminum compressors contributes very little to the polarization loss due to the short residence time in these compressors. Using the Nd:LMA laser at

4 W, our maximum OPC polarization during compression is  $\approx 65\%$  using a  $^4\text{He}:^3\text{He}$  mixture, which with  $f_{SC} = 0.81$ , we expect a maximum final polarization of  $\approx 52\%$ . Specifically, for a 46% polarized target, with a 5 bar·cm thickness, the neutron polarization, flipping ratio and total transmission at  $4 \text{ \AA}$  is 0.58, 3.8 and 0.29, respectively. We have recently constructed and tested a shielded transport solenoid which has transverse field gradients  $\approx 3 \times 10^{-4} \text{ cm}^{-1}$ . For a 1 bar sample of gas this gives  $T1_{field} \sim 1200 \text{ h}$ , and so the T1 of our MEOP cells in the solenoid will be dominated by wall relaxation.

### 6.3 Potential Improvements

Higher final polarizations,  $P_{SC} \approx 0.55$  are achievable with the compression system as it stands by replacing the Nd:LMA laser with an higher power Yb-fiber laser which has recently become commercially available [44]. To improve even further will require modification of the compression system, either by reworking the connecting tubing, or by increasing the volume and compression ratio of C2. We attribute the reduced T1 of the BC and the SC to the connecting tubing, which, in both cases, is a Pyrex region of high S/V, and thus increased relaxation. By reducing the length of these regions, we should be able to increase the T1, and thus the preservation. Increasing the volume and compression ratio of C2 would improve the preservation two-fold. First, the BC will be more efficiently drained and the SC will be more quickly filled, resulting in shorter fill times. Second, since the SC has a pressure dependent T1, by more rapidly increasing the SC pressure, the SC will more rapidly attain a longer T1. If the relaxation of the gas in the SC was dominated by the wall relaxation ( $T1 \sim 200 \text{ h}$ ), we estimate that the new preservation would be  $\approx 93 \%$ .

## 7 Acknowledgments

We thank IUCF for help with the infrastructure associated with the construction of the compressor system, especially the non-magnetic laser hut. We thank S.G.E. te Velthuis for her assistance with

the neutron transmission measurement taken on POSY I. We thank the IU glassblowing shops for fabricating the connecting tubing and the NIST glassblowing shop for fabricating the storage cells. This work has been supported by NSF CAREER grant PHY-9501312, by DOE grants DE-FG02-96ER45587 and DE-FG02-00ER45807 and NIST Interagency Agreements DE-A102-00ER45814.

## References

- [1] C. H. Tseng, G. P. Wong, V. R. Pomeroy, R. W. Mair, D. P. Hinton, D. Hoffmann and R. E. Stoner, F. W. Hersman, D. G. Cory, and R. L. Walsworth. Low-Field MRI of Laser Polarized Noble Gas. *Physical Review Letters*, 81:3785–3788, 1998.
- [2] M. Salerno, E.E. de Lange, T.A. Altes, J.D. Truwit, J.R. Brookeman, and J.P. Mugler III. Hyperpolarized  $^3\text{He}$  diffusion MRI of the lungs in emphysema: Comparison with pulmonary function tests –Initial experience. *Radiography*, 222:252–26, 2002.
- [3] S. Fичele. *Hyperpolarized  $^3\text{He}$  Gas Production for Magnetic Resonance Imaging of the Human Air-ways*. PhD thesis, University of Nottingham, 2002.
- [4] A.J. Deninger, B. Eberle, M. Ebert, T. Grossmann, et al. Quantification of regional intrapulmonary oxygen partial pressure evolution during apnea by He-3 MRI. *Journal of Magnetic Resonance*, 141:207–216, 1999.
- [5] D. Hussey, S. Fan, et al. Simultaneous Polarization Analysis of Zeeman Splitting in Polarized Neutron Reflectometry using a Polarized  $^3\text{He}$  Neutron Spin Filter. *Applied Physics A*, Supplement to A 74:S234–S236, 2002.
- [6] T.R. Gentile, G.L. Jones, A.K. Thompson, J. Barker, C.J. Glinka, B. Hammouda, and J.W. Lynn. SANS polarization analysis with nuclear-spin-polarized He-3. *Journal of Applied Crystallography*, 33:771–774, 2000.

- [7] J. Kulda, W. Heil, H. Humblot, F. Tasset, A. Wildes, V. Plakhty, E. Moskvina, P. Burette, J. Dreyer, and B. Fåk. Use of the  $^3\text{He}$  filter in search of the in-chain spin correlations in  $\text{YBa}_2\text{Cu}_3\text{O}_{6+x}$ . *Physica B*, 267-268:252–254, 1999.
- [8] W.M. Snow, A. Bazhenov, C.S. Blessinger, et al. Measurement of the parity violating asymmetry  $A(\gamma)$  in  $\vec{n}+p \rightarrow d+\gamma$ . *Nuclear Instruments & Methods in Physics Research A*, 440:729–735, 2000.
- [9] T.E. Chupp, R.J. Holt, and R.G. Milner. Optically pumped polarized H,D, and  $^3\text{He}$  gas targets. *Annual Review of Nuclear and Particle Science*, 45:373–411, 1994.
- [10] Z.E. Meziani. Polarized structure functions in the valence quark and resonance regions and the GDH sum. *Nuclear Physics A*, 721:118C–126C, 2003.
- [11] G. van der Steenhoven. The (spin) structure of the nucleon. *European Physical Journal A*, 18:377–381, 2003.
- [12] M. DeKieviet, D. Dubbers, C. Schmidt, D. Scholz, and U. Spinola.  $^3\text{He}$  Spin Echo: New Atomic Beam Technique for Probing Phenomena in the neV Range. *Physical Review Letters*, 75:1919–1922, 1995.
- [13] V. Druzhinina and M. DeKieviet. Experimental observation of quantum reflection far from threshold. *Physical Review Letters*, 91(193202), 2003.
- [14] B. Larson, O. Häusser, P.P.J. Delheij, D.M. Whittal, and d. Thiessen. Optical pumping of Rb in the presence of high-pressure  $^3\text{He}$  buffer gas. *Physical Review A*, 44:3108–3118, 1991.
- [15] F.D. Colegrove, L.D. Scheerer, and G.K. Walters. Polarization of  $\text{He}^3$  Gas by Optical Pumping. *Physical Review*, 132:2561–257, 1963.
- [16] W. Heil. Proceedings of the International Workshop on Polarized He-3 Beams and Gas Targets and Their Applications. Oppenheim, Germany, September 2002.

- [17] F.Tasset. Proceedings of the International Workshop on Polarized He-3 Beams and Gas Targets and Their Applications. Oppenheim, Germany, September 2002.
- [18] N.R.Newbury, A.S. Barton, G.D. Cates, W. Happer, and H. Middleton. Gaseous  $^3\text{He}$ - $^3\text{He}$  magnetic dipolar spin relaxation. *Physical Review A*, 48:4411–4419, 1993.
- [19] L.D. Schearer and G.K. Walters. Nuclear Spin-Lattice Relaxation in the Presence of Magnetic-Field Gradients. *Physical Review*, 139:A1398–A1402, 1965.
- [20] W. Fitzsimmons, L. Tankersly, and B. Walters. Nature of Surface-Induced Nuclear-Spin Relaxation of Gaseous  $\text{He}^3$ . *Physical Review*, 179:156–165, 1969.
- [21] Certain trade names and company products are mentioned in the text or identified in an illustration in order to adequately specify the experimental procedure and equipment used. In no case does such identification imply recommendation or endorsement by the National Institute of Standards and Technology, nor does it imply that the products are necessarily the best available for the purpose.
- [22] W. Franzen et al. *Review of Scientific Instruments*, 33:933, 1962.
- [23] D.R. Rich. *Investigation in the Development and Application of Optically Pumped Polarized  $^3\text{He}$  Neutron Spin Filters*. PhD thesis, Indiana University, 1999.
- [24] W. Lorenzon, T.R. Gentile, H. Gao, and R.D. McKeown. NMR calibration of optical measurement of nuclear polarization in  $^3\text{He}$ . *Physical Review A*, 47:468–479, 1993.
- [25] C. Larat. PhD thesis, Université Paris, 1991.
- [26] E. Stoltz, M. Meyerhoff, N. Bigelow, M. Leduc, P.J. Nacher, and G. Tastevin. High nuclear polarization in  $^3\text{He}$  and  $^3\text{He}$ - $^4\text{He}$  mixtures by optical pumping with a laser diode. *Applied Physics B*, 63:629–633, 1996.

- [27] T.R. Gentile and R.D. McKeown. Spin-Polarizing He-3 Nuclei with an Arc-Lamp-Pumped Neodymium-Doped Lanthanum Magnesium Hexaluminate Laser. *Physical Review A*, 47:456–467, 1993.
- [28] M. Leduc. Spin polarized  $^3\text{He}$ , A playground in many domains of physics. *Colloque de Physique*, 51:C6 317–331, 1990.
- [29] T.Y. Fan and M.R. Kokta. End-pumped Nd:LaF<sub>3</sub> and Nd:LaMgAl<sub>11</sub>)<sub>19</sub> lasers. *IEEE Journal of Quantum Electronics*, 25:1845–1849, 1989.
- [30] Tin P and L.D. Schearer. A High-power, Tunable, Arc-Lamp Pumped Nd-Doped Lanthanum-Hexaluminate Laser. *Journal of Applied Physics*, 68:950–953, 1990.
- [31] F. Bloch. Nuclear Induction. *Physical Review*, 70:460–474, 1946.
- [32] B.T. Saam and M.S. Conradi. Low frequency nmr polarimeter for hyperpolarized gases. *Journal of Magnetic Resonance*, 134:67–71, 1998.
- [33] E. Wildman. *Construction of a Portable NMR Device intended for use with  $^3\text{He}$* . Undergraduate Thesis, Hamilton College, 2001.
- [34] H.Y. Carr and E.M. Purcell. Effects of Diffusion on Free Precession in Nuclear Magnetic Resonance Experiments. *Physical Review*, 95:630, 1954.
- [35] T.R. Gentile, D.R. Rich, A.K. Thompson, W.M. Snow, and G.L. Jones. Compressing spin-polarized  $^3\text{He}$  with a modified diaphragm pump. *Journal of Research of the National Institute of Standards and Technology*, 106:709–729, 2001.
- [36] D.R. Rich, T.R. Gentile, T.B. Smith, A.K. Thompson, and G.L. Jones. Spin exchange optical pumping at pressure near 1 bar for neutron spin filters. *Applied Physics Letters*, 80:2210–2212, 2002.

- [37] W. Heil, H. Humblot, E. Otten, M. Schafer, R. Sarkau, and M. Leduc. Very long nuclear-relaxation times of spin-polarized He-3 in metal-coated cells. *Physics Letters A*, 201:337–343, 1995.
- [38] D.R. Rich et al. A measurement of the absolute neutron beam polarization produced by an optically pumped  $^3\text{He}$  neutron spin filter. *Nuclear Instruments and Methods in Physics Research A*, 481:431–453, 2002.
- [39] Amuneal Manufacturing Corp. *Magnetic Shield Design*.
- [40] J. Becker, W. Heil, B. Krug, M. Leduc, M. Meyerhoff, P.J. Nacher, E.W. Otten, Th. Prokscha, L.D. Schearer, and R. Surkau. Study of mechanical compression of spin-polarized  $^3\text{He}$  gas. *Nuclear Instruments and Methods A*, 346:45–51, 1994.
- [41] M. Batz, S. Baessler, W. Heil, E.W. Otten, D. Rudersdorf, J. Schmiedeskamp, Y. Sobolev, and M. Wolf.  $^3\text{He}$  spin filters for neutrons. *Journal of NIST*.
- [42] F. Tasset, W. Heil, H. Humblot, E. Lelièvre-Berna, and T. Roberts. The  $^3\text{He}$  neutron spin filter at ILL. Technical report, ILL, 1996.
- [43] T.W. Roberts, H. Hmbolt, F. Tasset, E. Lelièvre-Berna, A.R. Wildes, A. Ivanov, A.K. Petoukhov, L.-P. Regnault, A.D. Hillier, J. Kulda, J.R. Stewart, M. Thomas, P. Malbert, D. Jullien, Y. Gibert, R. Gay, E. Bourgeat-Lami, and r. Chung. The current status of the  $^3\text{He}$  neutron spin filter (nsf) project at the ill. *Physica B*, 297:282–287, 2001.
- [44] We are aware of two companies, KEOPSYS and IGP.
- [45] T. Prokscha. PhD thesis, Universität Mainz, 1991.

## List of Figures

1	Compressor schematic . . . . .	29
2	Front view of compressor system . . . . .	30
3	C1 valve timing sequence . . . . .	31
4	Pressure in compressor system volumes during a fill to $\sim 1.20$ bar . . . . .	32
5	Optical Pumping Rate in the OPCs . . . . .	33
6	NMR-FID schematic diagram . . . . .	34
7	Typical BC and SC FID signals . . . . .	35
8	$^3\text{He}$ polarization and pressure dependence of the OPC-FID signal . . . . .	36
9	Relaxation rate for C2 . . . . .	37
10	BC polarization relaxation and preservation data . . . . .	38
11	Schematic diagram of the POSY neutron reflectometer . . . . .	39
12	Depolarized $^3\text{He}$ neutron transmission . . . . .	40
13	Neutron transmission through polarized cell . . . . .	41

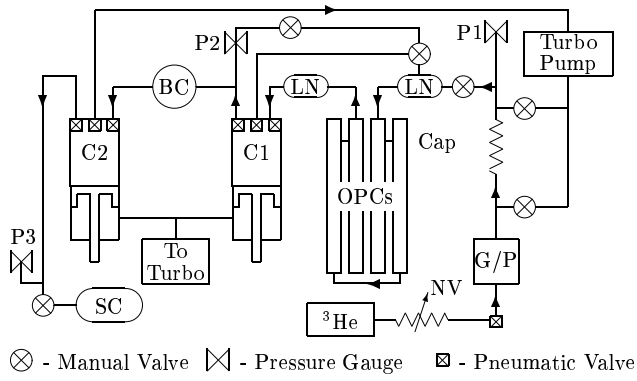


Figure 1: Schematic of the compressor system. Arrows indicate  $^3\text{He}$  flow while compression is in progress. The labeled system components are: storage cell (SC), buffer cell (BC), optical pumping cells (OPCs), compressors (C1, C2), pressure transducer (P1), non-magnetic strain gauges (P2, P3), needle valve (NV), getter/purifier (G/P), capillary tubing (Cap.), and liquid nitrogen traps (LN).

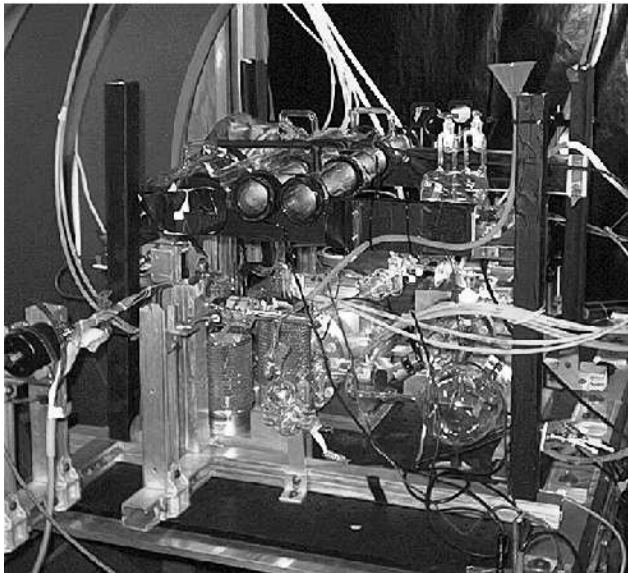


Figure 2: Photograph of the IUCF  $^3\text{He}$  compressor system. Going clockwise around the photo: the optical pumping cells in the top center, the Rb coated storage cell Orion, the aluminum holding blocks for C2, the buffer cell, part of the flange of C1, the two LN cold traps, and the Baratron pressure transducer is in the far left. The posts are aluminum Uni-Strut covered in black tape to reduce reflection of the light from the discharge.

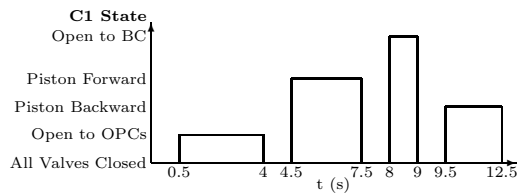


Figure 3: Valve sequence of C1. Closed means that C1 is closed to all other volumes. The 0.5 s delay between valve or piston operations is to ensure that there is no overlap between successive operations. The timing sequence for C2 is similar with  $OPC \rightarrow BC$  and  $BC \rightarrow SC$ , the main difference being that during the filling of the BC, C2 is exposed to the turbo-pump to evacuate the residual gas from the previous BC drain.

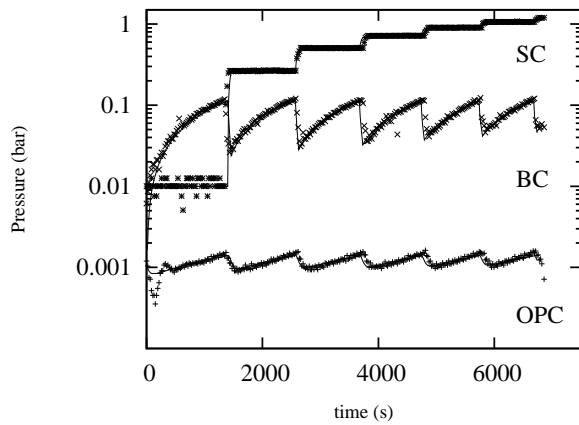


Figure 4: Measured pressure in the BC and SC and the corrected pressure in the OPC during a fill to 1.20 bar. The solid black lines are the simulated pressures based on the gas flow rate. The spread in the pressure data for the OPC is due to the pressure fluctuations when the inlet to C1 is opened and closed. The pressure measured for the OPC is higher than that predicted by the simulation since a pressure gradient must exist in order for there to be a gas flow. The average pressure difference between the model and the measured pressure is  $\approx 0.1$  mbar and is in agreement with the flow rate of the system and is used to correct the measured OPC pressure and optical polarimeter pressure calibration coefficients. With this correction, the simulation correctly predicts the time dependence of the pressure in the OPCs, BC and SC.

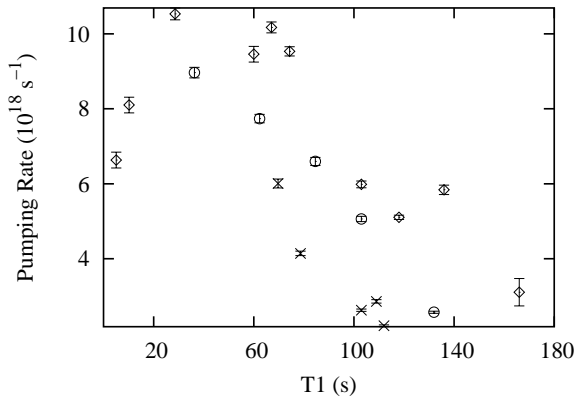


Figure 5: Optical pumping rate ( $\text{nuclei}\cdot\text{s}^{-1}$ ) of pure  $^3\text{He}$  in one of the OPCs as a function of RF discharge as characterized by the relaxation time (T1). The laser power was 4.0 W with both the 0.3 and 1.0 mm etalons in the laser cavity. The  $^3\text{He}$  polarization was measured by the optical polarimeter, discussed below. The (×) are for a pressure of 1 mbar, the (⊙) are for 1.26 mbar and the (◇) are for a pressure of 1.43 mbar. The pumping rate was determined by fitting the polarization accumulation using equation 4. The relaxation time was determined by shuttering the laser and measuring the subsequent polarization decay over a period of 90 s. The limited discharge strength range for the lower pressures is due to the difficulty of maintaining a weak discharge. These data are in qualitative agreement with those reported in [27].

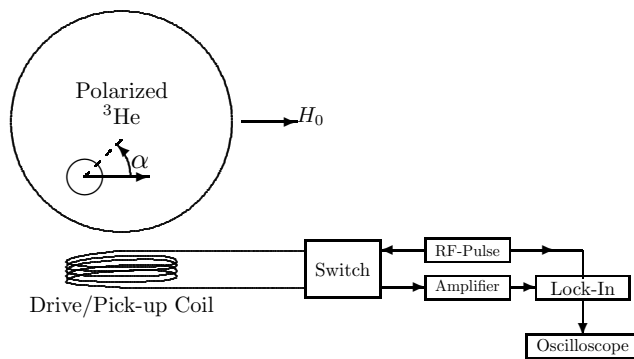


Figure 6: Schematic diagram of the NMR-FID gauge. The RF-pulse creates a rotating field, which tips the spins of the polarized nuclei an angle  $\alpha$  w.r.t to the polarization axis. The precession of the transverse component of the magnetization induces an EMF in the drive coil. This EMF is sent to a lock-in amplifier whose reference frequency is that of the initial drive pulse. The output of the lock-in is then the beating between the Larmor frequency and the drive pulse and is acquired on a digital oscilloscope.

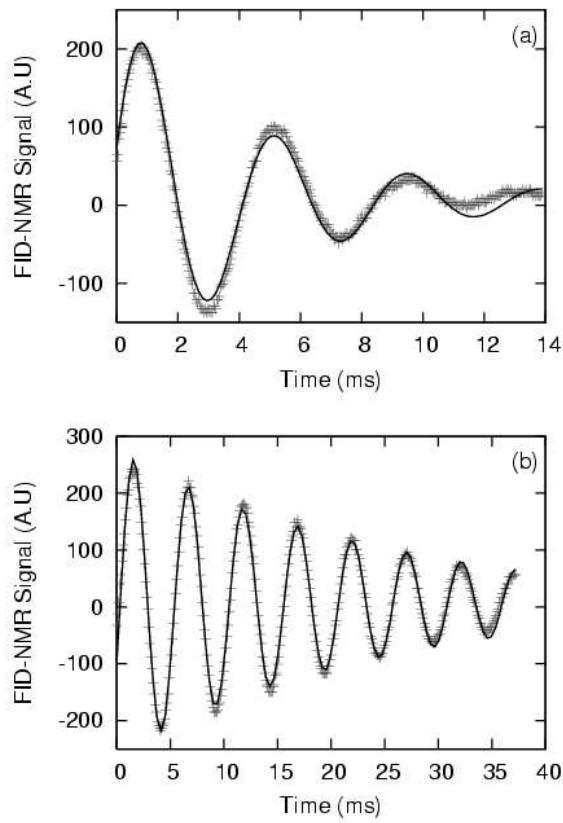


Figure 7: Typical FID signal obtained in the BC at a pressure of 54 mbar (a) and in the SC for a pressure of 1.16 bar (b). The solid line is a fit to the data assuming an exponentially damped sinusoid. The BC signal corresponds to 54 mbar of pure  $^3\text{He}$  polarized to 32%. The SC signal corresponds to 1.16 bar of a 2:1  $^4\text{He}$ : $^3\text{He}$  mixture with a polarization of 32%.

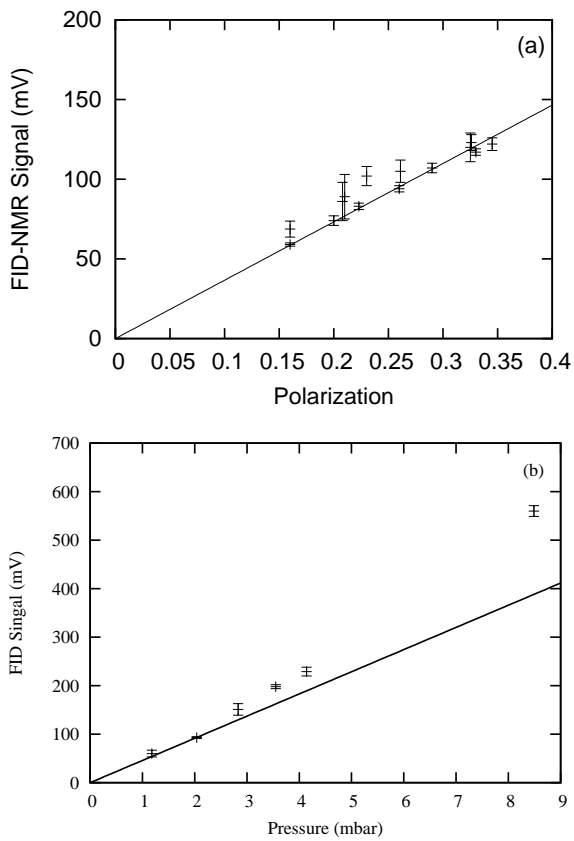


Figure 8:  $^3\text{He}$  FID polarimetry in the OPCs. (a) FID signal vs. polarization as determined by the polarimeter. The curve is a linear best fit to the data. (b) FID signal vs. pressure for constant polarization. Polarized gas was compressed into the buffer cell and then bled into the OPC in pressure intervals as indicated. The line is a fit to the first two data points to demonstrate the FID signal is non-linear in the pressure as expected.

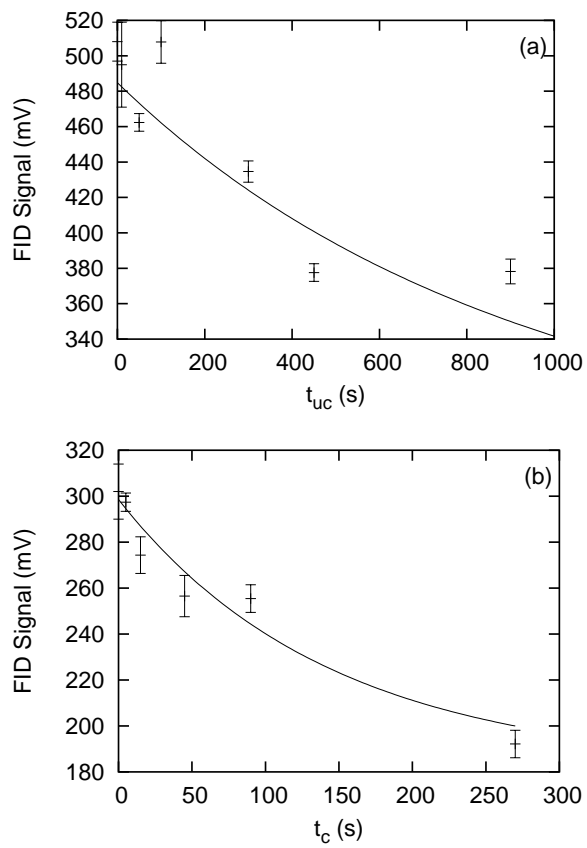


Figure 9: Data for the time dependence of the  $^3\text{He}$  polarization in the withdrawn (a) and forward (b) piston positions of C2.  $T1_{u,(uc)}$  were obtained by fits of Equation 6 to the data.

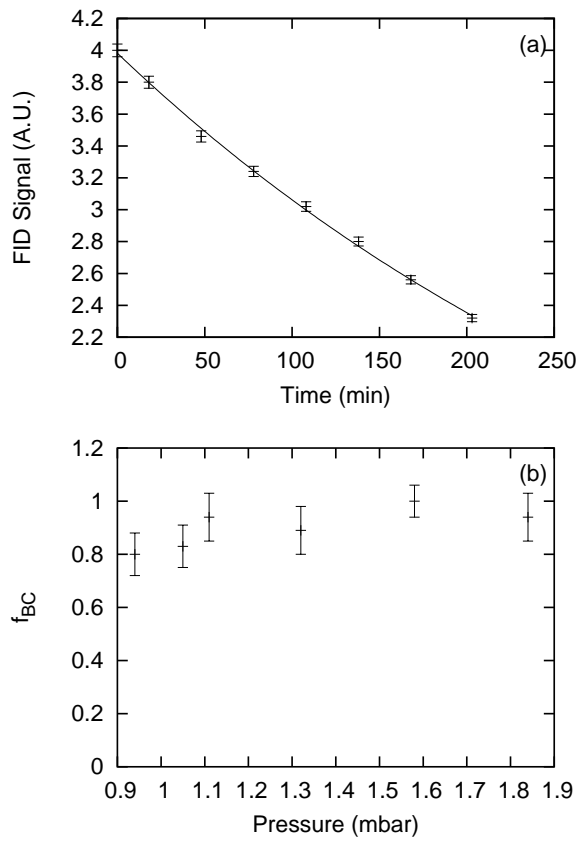


Figure 10: Relaxation and preservation data for the BC. (a) Representative plot of the polarization vs. time for the BC. The data corresponds to 52 mbar of pure  $^3\text{He}$  in the BC, and the  $T_1$  from the fit is  $6.5 \pm 0.2$  hours. (b) Polarization preservation for filling the BC as a function of the average pressure in the optical pumping cells during compression to 65 mbar. The average of all  $f_{BC}$  is  $0.92 \pm 0.05$ , with the uncertainty coming from the r.m.s. deviation of the distribution.

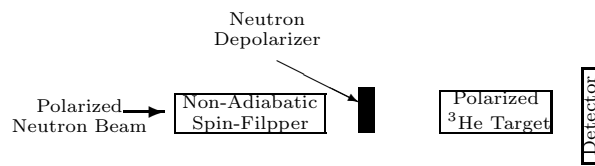


Figure 11: Experimental setup with the polarized target of  $^3\text{He}$  in the POSY I beam line, not drawn to scale. The neutron depolarizer was a bulk sample of iron that had randomly oriented magnetic domains. The depolarizer was used so as to not include the polarization properties of the supermirror nor the spin transport of the instrument in the analysis, as well as to not have to remove the supermirror.

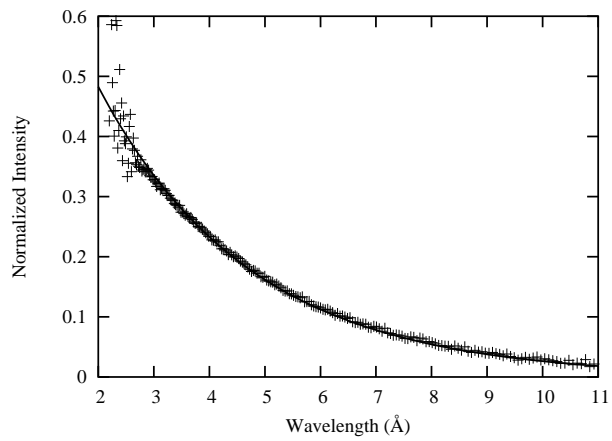


Figure 12: Neutron transmission through the depolarized target, normalized by the transmission through the empty cell. The exponential fit gives the  $^3\text{He}$  thickness,  $n l = 5.040 \pm 0.004\text{bar}\cdot\text{cm}$ .

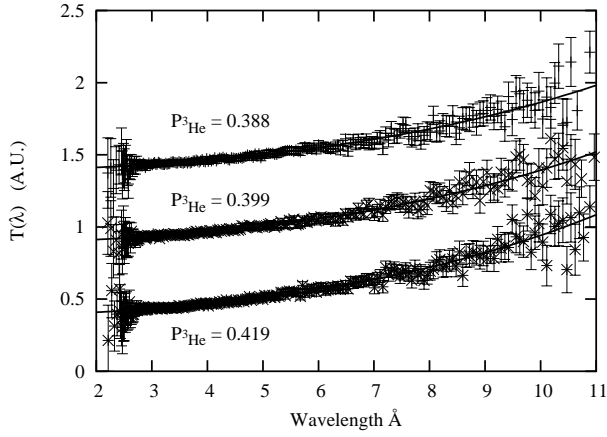


Figure 13: Neutron transmission through the polarized cell at three different times, normalized by the transmission through the depolarized cell. The transmissions for the different polarizations are offset by 0,0.5,1 from top to bottom for clarity. The three transmissions were taken over four hours each, and the times after Orion was transferred to the transport solenoid to which they correspond are  $P(6.35 \text{ h}) = 0.419 \pm 0.003$ ,  $P(11.35 \text{ h}) = 0.399 \pm 0.003$  and  $P(15.35 \text{ h}) = 0.388 \pm 0.004$ . From the time dependence of the polarization, Orion's T1 in the solenoid was determined to be  $100 \pm 10 \text{ h}$ . This relaxation time implies that immediately after compression, the  $^3\text{He}$  polarization was  $0.457 \pm 0.046$ , yielding a polarization preservation of  $f_{SC} = 0.81 \pm 0.09$ .

## List of Tables

1	Approximate relaxation times in the presence of given materials for $S/V \approx 1 \text{ cm}^{-1}$ . .	43
2	FID Calibration coefficients . . . . .	44
3	Summary of relevant quantities for the compressor system's volumes . . . . .	45

Material	$T_{wall}$	$\eta$ ( $s^{-1}cm$ )
Titanium	72 min	$2.3 \times 10^{-4}$
Aluminum	620 min	$2.8 \times 10^{-5}$
Pyrex	$\approx 60$ min	$2.8 \times 10^{-4}$
Corning 1720, 7056	$\approx 20$ h	$1.4 \times 10^{-5}$
Viton o-ring	14 min	$1.2 \times 10^{-3}$
Krytox grease*	$\approx 1$ min	$1.7 \times 10^{-2}$

Table 1: Approximate relaxation times and respective  $\eta$  in the presence of given materials for  $S/V \approx 1 \text{ cm}^{-1}$  [45]. \*The value for Krytox has not been measured directly, but rather inferred in simulations of relaxation mechanisms discussed in [23].

Coil	Pressure (mbar)	$\kappa_{AB}$ (mV/mbar)	$\kappa_{BC}$ (mV/mbar)
OPC	2.0	$260 \pm 20$	$210 \pm 11$
BC	65	$23.7 \pm 0.7$	$22.8 \pm 0.7$
SC	925	$1.32 \pm 0.03$	$1.18 \pm 0.03$

Table 2: Results of a calibration procedure as described in the text. The calibration coefficients for the OPC and BC are for pure  $^3\text{He}$  gas, while for the SC they are for a mixture of 2:1  $^4\text{He}:^3\text{He}$ .

Region	Material	Volume (cm <sup>3</sup> )	T1	Preservation
OPCs	Pyrex	7050 ± 50	(150±9) min	1.00
C1	6061-T6 Al	2615 ± 50	(60±3) min / ((3.0±0.2) min)	.99
Buffer	Corning 1720	1107 ± 30	(290±10) min	.92±0.05
C2	6061-T6 A	725 ± 50	(37±2) min / ((2.1±0.7) min)	.99
SC, CT	GE180, Pyrex	480 ± 20	(8.6±1.1) h (at 170 mbar)	0.89
Orion	GE180	474 ± 20	(210 ± 10) h	n/a

Table 3: The compressor system's major components' physical parameters. Relaxation times for the compressors are for the piston in the withdrawn(forward) position. Preservation is the estimated contribution to the loss of the <sup>3</sup>He polarization during the compression cycle. The preservation for the compressors is based on the estimate discussed in Section 5.1, while those for the BC and the exposed SC (SC,CT) are the measured quantities discussed in Section 5.3. Orion's isolated T1=210 h was measured at a pressure of 0.933 bar of pure <sup>3</sup>He.